IR-Induced Second Harmonic Generation in $Sb_2Te_3-BaF_2-PbCl_2$ Glasses

I. V. Kityk*

Institute of Physics WSP, University of Czestochowa, Al. Armii Krajowej 13/15, PL-42201 Czestochowa, Poland, and Institute of Computer Modeling, University of Technology, Krakow, ul. Warszawska 24, Krakow, Poland

Received: January 15, 2003

Theoretically predicted and experimentally confirmed occurrence of infrared-induced second harmonic generation for glasses in the middle infrared spectral region is described by fifth-order nonlinear optical susceptibility. This effect is observed in the middle-IR region when the value of the electronic energy gap is comparable to the energies of actual phonons participating in the anharmonic (noncentrosymmetric) electron−phonon interactions. As a subject for the investigations, $Sb_2Te_3-BaF_2-PbCl_2$ glasses were chosen because they are transparent in the spectral range of 0.8−10.1 μm. The second harmonic generation (SHG) output signal within the 1.5−4.8 μm spectral range demonstrated a significant spectral dependence. Correlation of the SHG spectral dependences with spectral positions of the anharmonic phonon frequencies confirms that the fifth-order steady-state process occurs as a result of both the cascading processes and IR-induced charge density noncentrosymmetry. A maximum value of the SHG is achieved at a pump−probe delay time of about 20 ps, which is typical for the anharmonic electron−phonon interactions.

1. Introduction

It is well-known that second-order nonlinear optical effect in glasses such as second harmonic generation (SHG) and linear electrooptics effects (LEOE) are generally forbidden by symmetry.[1] An external electric field is usually applied to induce noncentrosymmetry (electroinduced second-order effects).[2] Unfortunately, this method fails for infrared (IR) materials, which are transparent in the middle-IR because of high electroconductivity of the materials. However, the operation of glasses in the middle-IR spectral range is very important for development of the IR optical fibers for CO lasers.[3]

For the reasons presented above, IR optical poling[4] in glasses becomes increasingly attractive because it offers the possibility of creation of optically operated waveguides for recording and transmission of IR information. To date, all investigations, including those in the femtosecond regime, were performed for the near-IR (less than 2 μm) wavelengths.[5,6] Among the IR materials, chalcohalide and chalcogenide glasses[7−9] are very promising. Photoinduced effects in the chalcogenide glasses are well studied for the visible and near-IR spectral ranges.[9] However, the physical origin of the photoinduced second-order nonlinear optical properties is significantly different when the middle-IR spectral range is considered. For this spectral range, we have a comparability of the IR frequencies and phonon frequencies of the glasses.[8] As a consequence, one can expect significant contribution of optically induced electron−phonon interactions (EPI) to second-order nonlinear optical susceptibilities.[8] The EPI are described by third-order space derivatives of the electrostatic potential[10] and appear due to relatively high photoinducing power densities (up to 0.6 GW/cm^2). Thus in this case, the second-order nonlinear optical effects might be significant.[11] However, following general phenomenological consideration,[1,2] one can expect a necessity to introduce nonlinear optical susceptibilities of higher orders.

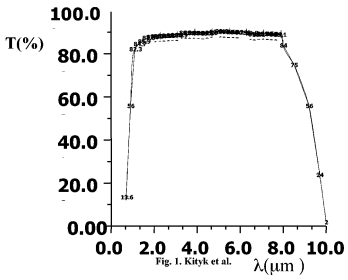

Figure 1. Transparency of the $Sb_2Te_3-BaF_2-PbCl_2$ glass.

In the present paper, a new type of IR optical poling consisting of IR photopumping of appropriate electronic states using the pulsed IR parametric generation operating within the 4−10.1 μm spectral range is proposed. A novel nonlinear optical effect consisting of the IR-induced lattice-electron poling (phototransient effect) and fifth-order cascading steady-state process described by fifth-order nonlinear optical (NLO) tensor is revealed. As a consequence, IR-induced noncentrosymmetry is observed in the electronic charge density distribution of a particular glass.

Similar to the traditional all-optical poling technique,[12] the method consists of three basic physical principles: a net orientation of particular molecular clusters, a photoexcited resonance-selective excitation, and an electric field induced SHG. In the case of the IR optical poling, the photoinduced noncentrosymmetry plays a crucial role and is enhanced because of the occurrence of the electron−phonon steady-state processes, which satisfy the phase-matching conditions within the larger range of angles.

For the investigations, we have chosen $Sb_2Te_3-BaF_2-PbCl_2$ glasses because they are transparent within the spectral range of 0.7−10.1 μm (see Figure 1), where many industrial IR lasers operate.[8] They are also relatively homogeneous and possess good photo- and thermomechanical properties, and their fabrica-

* E-mail: kityk@torus.uck.pk.edu.pl.

10.1021/jp030058a CCC: $25.00
Published on Web 08/23/2003

tion is technologically relatively simple.[13] The investigated glasses were synthesized by a technique similar to that described in ref 8.

In section 2, phenomenological and microscopic description of the phenomenon observed are presented. Section 3 describes the obtained data together with an appropriate discussion.

2. Theoretical Approach

The noncentrosymmetric photoinduced electron−phonon anharmonicity requires participation of at least three phonons. So the photoinduced SHG effect may be described phenomenological by an expression

$$P_i = \chi_{ijklmn} \cdot \mathbf{E}_j^{(\omega)} \cdot \mathbf{E}_k^{(\omega)} \cdot \mathbf{E}_l^{(\Omega_1)} \cdot \mathbf{E}_m^{(\Omega_2)} \cdot \mathbf{E}_n^{(\Omega_3)} \quad (1)$$

where χ_{ijklmn} is fifth-order NLO susceptibility; $\mathbf{E}_l^{(\Omega_1)}$, $\mathbf{E}_m^{(\Omega_2)}$, and $\mathbf{E}_n^{(\Omega_3)}$ are effective electric strengths corresponding to interacting photoinduced phonons (created by photoinduced electrostriction effect) participating in the anharmonic EPI process and causing ionic displacive polarization, and $\mathbf{E}_k^{(\omega)}$ and $\mathbf{E}_j^{(\omega)}$ are effective electric strengths of the IR beams with polarization k and j, respectively.

Quantum chemical calculations of matrix dipole moments were done, as well as eigenenergies, to simulate dependencies of the observed SHG versus pump−probe delay time and pump power (see eq 1). A detailed description of the calculation technique is presented in the ref 8. Calculations were done considering both traditional formalism of second-order susceptibility, $\chi_{ijk}^{(2\omega)}$ (pure electronic two-photon cascading process), as well as higher-order steady-state EPI processes described by six rank tensors. Equations 2a and 2b describe these processes, respectively:

$$\chi_{ijk}^{(\omega,\omega)} = \frac{1}{\hbar^2}\frac{e^3 N}{2!}\hat{P}_{ijk}\sum_k\sum_{\alpha,\beta}\left[\frac{\langle 0|i|\alpha\rangle\langle\alpha|j|\beta\rangle\langle\beta|k|0\rangle}{(2\omega+\omega_\alpha)(\omega+\omega_\beta)} + \frac{\langle 0|j|\alpha\rangle\langle\alpha|i|\beta\rangle\langle\beta|k|0\rangle}{(\omega_\alpha-2\omega)(\omega_\beta-\omega)} + \frac{\langle 0|j|\alpha\rangle\langle\alpha|k|\beta\rangle\langle\beta|i|0\rangle}{(\omega+\omega_\beta)(\omega_\alpha-\omega)}\right] \quad (2a)$$

$$\chi_{ijklmn}^{(\omega,\omega,\Omega_1,\Omega_2,\Omega_3)} =$$

$$\frac{1}{\hbar^3}N\hat{P}\sum_k\sum_{\alpha,\beta,\gamma,\delta,\eta,\theta}\left[\frac{\langle 0|i|\alpha\rangle\langle\alpha|j|\beta\rangle\langle\beta|k|\gamma\rangle\langle\gamma|l|\delta\rangle\langle\delta|m|\eta\rangle\langle\eta|n|0\rangle}{(\omega_{\gamma 0}-2\omega-\Omega_1-\Omega_2-\Omega_3)(\omega_{\delta 0}-2\omega)(\omega_{\eta 00}-\omega)_{\gamma 0}(\omega_{\beta 0}-2\omega-\Omega_1)(\omega_{\alpha 0}-2\omega-\Omega_1-\Omega_2)}\times\right.$$

$$\frac{\langle 0|i|\alpha\rangle\langle\alpha|j|\beta\rangle\langle\beta|k|\gamma\rangle\langle\gamma|l|\delta\rangle\langle\delta|m|\eta\rangle\langle\eta|n|0\rangle}{(\omega_{\gamma 0}+2\omega)(\omega_{\delta 0}-\omega)(\omega_{\eta 00}-\omega)_{\gamma 0}(\omega_{\beta 0}-2\omega-\Omega_1)(\omega_{\alpha 0}-2\omega+\Omega_1+\Omega_2)}+$$

$$\frac{\langle 0|i|\alpha\rangle\langle\alpha|j|\beta\rangle\langle\beta|k|\gamma\rangle\langle\gamma|l|\delta\rangle\langle\delta|m|\eta\rangle\langle\eta|n|0\rangle}{(\omega_{\gamma 0}-2\omega-\Omega_1)(\omega_{\delta 0}-2\omega)(\omega_{\beta 0}+2\omega-\Omega_2)(\omega_{\alpha 0}-2\omega+\Omega_1-\Omega_2)}+$$

$$\frac{\langle 0|i|\alpha\rangle\langle\alpha|j|\beta\rangle\langle\beta|k|\gamma\rangle\langle\gamma|l|\delta\rangle\langle\delta|m|\eta\rangle\langle\eta|n|0\rangle}{(\omega_{\gamma 0}-2\omega+\Omega_3)(\omega_{\delta 0}-2\omega)(\omega_{\eta 00}+\omega)_{\gamma 0}(\omega_{\beta 0}+2\omega-\Omega_3)(\omega_{\alpha 0}-2\omega+\Omega_1+\Omega_2)}+$$

$$\frac{\langle 0|i|\alpha\rangle\langle\alpha|j|\beta\rangle\langle\beta|k|\gamma\rangle\langle\gamma|l|\delta\rangle\langle\delta|m|\eta\rangle\langle\eta|n|0\rangle}{(\omega_{\gamma 0}-2\omega-\Omega_1+\Omega_2-\Omega_3)(\omega_{\delta 0}+2\omega)(\omega_{\eta 00}-\omega)_{\gamma 0}(\omega_{\beta 0}-2\omega-\Omega_1)(\omega_{\alpha 0}+2\omega-\Omega_1)(\omega_{\alpha 0}+2\omega+\Omega_1-\Omega_2)}+$$

$$\left.\frac{\langle 0|i|\alpha\rangle\langle\alpha|j|\beta\rangle\langle\beta|k|\gamma\rangle\langle\gamma|l|\delta\rangle\langle\delta|m|\eta\rangle\langle\eta|n|0\rangle}{(\omega_{\gamma 0}+2\omega+\Omega_1+\Omega_2+\Omega_3)(\omega_{\delta 0}+2\omega)(\omega_{\eta 00}+\omega)_{\gamma 0}(\omega_{\beta 0}+2\omega+\Omega_1)(\omega_{\alpha 0}+2\omega+\Omega_1+\Omega_2)}\right] \quad (2b)$$

where $\langle\alpha,\beta...|i,j,...|\delta...\rangle$ are transition dipole moments between particular electron and electron−phonon quantum levels α, β, δ... for polarization components $i,j,...$; $\omega_{m,n}$ are mean frequencies of quantum transitions between the electron and EPI phonon states (for example, m and n in the present case). Ω_1, Ω_2, and Ω_3 are frequencies of the IR phonons with polarization 1, 2, and 3, respectively. In this case, we permuted all of the possible signs in the phonon states. This fact reflects a second-order virtual level interaction between the quantum virtual levels.[1,2]

Following cluster self-consistent norm-conserving pseudopotential calculations (for details see ref 8) within the plane-wave basis set for glasses, one can predict the spectral behavior of the fifth- and second-order NLO effects. From Figure 2, one can see that only consideration of the electron−phonon anharmonicity (see curve 2) could give a substantial output SHG signal compared with the pure electronic cascading process (curve 1). The intensity of the output SHG signal caused by pure electronic contribution should be equal to about $10^{-6}-10^{-7}$ with respect to the fundamental ones. Only the anharmonic phonon subsystem gives a contribution at least two orders higher.

The calculations were carried out using the quantum-chemical computer package HYPERCHEM 7.0. They showed that the Sb−Te chemical bonds play the main role in the observed photoinduced nonlinear optical susceptibilities. For Ba−F and Pb−Cl bonds, IR-induced changes are relatively small (less than 1.42%). In particular, the matrix dipole moments for the Sb−Te bonds are equal to about 8.39 D, while for the Ba−F and Pb−Cl bonds, the total dipole moments are equal to 0.18 and 0.91 D, respectively. The interaction of the fundamental CO_2 laser beam, $E_{pr}^{(\omega)}(r,t)$, with the investigated medium may be described as follows:

$$E(r,t) = E_{pr}^{(2\omega)}(r,t) + E_{pr}^{(\omega)}(r,t) + E_{pump}^{(\omega_p)}(r,t) + E^{(\Omega_1\pm\Omega_2\pm\Omega_3)}(r,t-\tau) \quad (3)$$

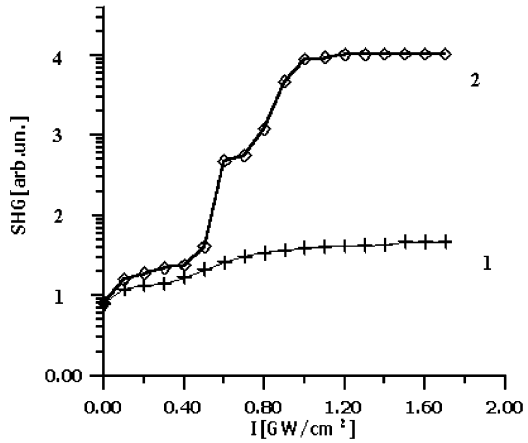

Figure 2. Calculated dependences of the IR-induced SHG: (+) within a framework of taking into account of the pure electronic sub-system; (◇) within a framework of the EPI contribution.

where τ is a pump−probe delay time and indices pump and pr correspond to pumping and probing IR beams, respectively. The interacting photons are presented in the plane wave approximation:

$$E_{pr}^{(\omega)}(r,t) = E^{(0)} \exp[i(\omega t + k\mathbf{r} + \phi_1)] \quad (4)$$

where $E^{(0)}$ and ϕ_1 are amplitude and phase of the electromagnetic probe wave, respectively, and possess the frequency ω at instant time t and the point of space **r**.

A term with the frequency of 2ω is caused by photoinduced noncentrosymmetry and is similar to process of interference for two coherent waves with the fundamental and doubled frequencies (optical poling).[17] The temporarily averaged output nonlinear polarization for the doubled frequency may be expressed in a form

$$P^{(2\omega)}(r) \cong \epsilon_0 |E_{pr}^{(\omega)}(r,t-\tau)|^2 \{\langle E_{pump}^{\omega_p}(r,t)[E^{\Omega_1\pm\Omega_2\pm\Omega_3}(r,t)]^2\rangle + \langle E_{pr}^{\omega}(r,t)[E^{\Omega_1\pm\Omega_2\pm\Omega_3}(r,t)]^2\rangle\langle E_{pr}^{2\omega}(r,t-\tau)[E^{\Omega_1\pm\Omega_2\pm\Omega_3}(r,t)]^2\rangle\} \quad (5)$$

where the broken brackets mean averaging over time.

The first term corresponds to interaction between the pumping CO laser beam and the modulated photoexcited one with noncentrosymmetric charge density distribution due to IR-induced anharmonic phonon modes possessing combined frequencies $\Omega_1 \pm \Omega_2 \pm \Omega_3$. These terms are responsible for appearance of the photoinduced noncentrosymmetry at the given point of the medium (**r**). The amplitudes of the photoinduced anharmonic displacive modes, $E^{(\Omega_1\pm\Omega_2\pm\Omega_3)}(r,t)$, are proportional to the IR-inducing power. From the general phenomenological consideration of the particular cluster, one can conclude that the SHG output will be maximal for parallel polarization directions for both the pumping and fundamental beams. This one reflects the fact that direction of the anharmonic charge density shift should be parallel to the direction of the pumping beam polarization.

Another condition is connected with satisfying of phase-matching requirements that, in the case of the fifth-order cascading process, are fulfilled in the larger angle range compared with the traditional second-order SHG. The second-order noncentrosymmetric effect may be observed because there exists a range of phonon frequencies satisfying conditions $\omega - \omega_1 \pm n\Omega_1 \pm g\Omega_2 \pm h\Omega_3 = 0$ (n, g, $h = \pm1, \pm2, \pm3, ...$), which are necessary for appearance of noncentrosymmetric tensor components during the IR picosecond photoexcitation.

When we consider the fifth-order cascading nonlinear interactions, it is necessary to consider interactions between the fundamental ($k_{pr}^{(\omega)}$), doubled frequency ($k^{(2\omega)}$), and the pumping $k_{pump}^{(\omega_p)}$ beams and the corresponding photoinduced combined anharmonic frequencies with wave vectors ($\mathbf{K}^{(\Omega_1\pm\Omega_2\pm\Omega_3)}$). As a consequence, we obtain a wide range of angles satisfying the phase-matching conditions:

$$P^{(2\omega)}(r,t) \cong \epsilon_0 \chi^{(5;2\omega)}(2\omega;\omega,\omega,\Omega_1,\Omega_2,\Omega_3)|E_{pr}^{(\omega)}(r,t)|^2 \exp[-i\Delta k r] \quad (6)$$

where $\Delta k = k^{(2\omega)} - k_{pr}^{(\omega)} \pm (k_{pump}^{(\omega_p)} + \mathbf{K}^{(\Omega_1\pm\Omega_2\pm\Omega_3)})$.

The range of angles satisfying the phase-matching conditions should be relatively wide because there exist large numbers of phonon modes satisfying these conditions within the spectral range 0.8−4 μm. The calculated dependences of the SHG intensities versus the IR pump power are presented in Figure 1. The results of the calculations predict substantial increase of the IR-induced SHG with increasing IR pump power densities.

3. Results and Discussion

The experimental setup allows performance of the measurements of the IR-induced SHG and is similar to that described in the ref 8. The pulsed CO laser beam ($\lambda = 5.5$ μm; $P = 12-28$ MW; $\tau = 0.44-80$ ps, frequency repetition 8−15 Hz) serves as an IR pumping signal. ZnSe and proustite (Ag_3AsS_3) single crystals are used as optical parametrical generators (OPG) operating in the wide spectral range.

Picosecond mode-locked CO_2 laser beam ($\lambda = 10.6$ μm; $P = 25$ MW; $\tau = 2-10$ ps) is used as a fundamental (probing) beam. The laser beam was temporarily synchronized with the pump CO laser beam ($\lambda = 5.5$ μm) and with the optical parametrical generators (OPG). An IR cooled fast-response detector with an electronic boxcar integrator (gain time up to 420 ps) was used for detection of the SHG output signal at different incident angles of the fundamental beam. Photoinduced birefringence was taken into account for correct evaluation of the photoinduced phase-matching conditions.

The incident angles of the fundamental beams were changed within the −60° to 60° range. The ratio of the SHG output intensity to the incident fundamental beam intensity was equal roughly to $10^{-2}-10^{-3}$. The $\chi^{(5)}$ tensor values were evaluated from eq 6 with accounting of Fresnel losses, Gaussian-like space sequence profile of the beam, optical attenuation, and the photoinduced birefringence. A fluorescence signal was observed below 1.2 μm wavelengths. This one allowed separation of the spectrally doubled frequency SHG output signal from the light scattering noise using a grating IR monochromator with spectral resolution of about 7 nm/mm. The proper time duration of the SHG signal was equal to about 1.2 ps. Statistic of the SHG output signals was chosen to satisfy the Student statistical test with accuracy better than 0.03. Only slight phonon modes within the 0.8−5.0 μm spectral range were observed. In agreement with the theoretical predictions, the increasing IR-inducing beam powers favored increasing intensities of the corresponding IR modes.

In Figure 3, experimental dependencies of the fifth-order SHG intensities (proportional to $\chi^{(5;2\omega)}$) versus the IR laser pump power density (at $\lambda = 5.5$ μm) (calculated from the eq 6) are presented. An increase of the IR-induced SHG with the increasing IR pump power (within the 0−0.8 GW/cm^2 range) is observed. As temperature rises, the values of the photoinduced SHG signal increase up to 2×10^{-40} m^4/V^4. The SHG signal

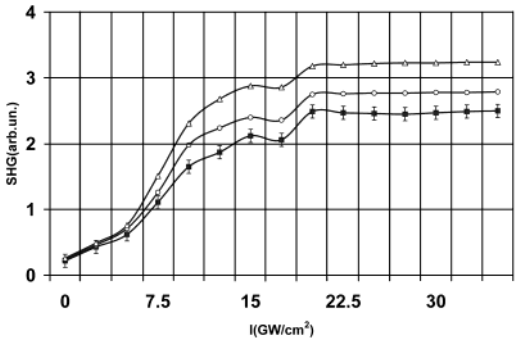

Figure 3. Dependence of the fifth-order nonlinear optical susceptibility, $\chi^{(5)}$, versus IR-induced power density at different temperatures: (△) 77 K; (○) 100 K; (■) 300 K. All of the measurements were done for the fundamental wavelength, 9.1 μm.

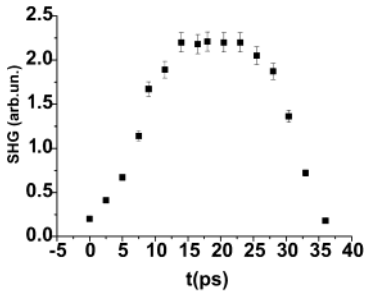

Figure 4. Typical dependence of the IR-induced SHG output signal versus pump−probe delaying time.

reaches a saturation point for the IR pumping power densities at about 0.8 GW/cm^2. The values of diagonal tensor component $\chi^{(2\omega)}_{xxxxx}$ are at least 1 order of magnitude larger than that of the off-diagonal tensor component. Photochemical destruction processes are observed for the pump power densities higher than 1.0 GW/cm^2, including irreversible ones. The calculated SHG signal is presented in Figure 2. This one unambiguously shows a fact that only appropriate accounting of the photoinduced anharmonic EPI (stimulated by electrostriction processes) allows description of the observed experimental SHG dependences appropriately.

Another fact confirming the significant role of the anharmonic EPI consists of a dependence of the SHG intensity versus the pump−probe delay time (see Figure 4). One can clearly see that the SHG maximal signal is observed for the pump−probe delay times equal roughly to 15−25 ps, which is typical for relaxation times for the anharmonic EPI.

One of differences of the IR poling compared with the pure optical poling consists of comparable values of IR-induced electronic and phonon dipole moments contributing to the nonlinear optical susceptibilities.

To confirm steady-state cascading processes, the SHG spectral dependence was measured (see Figure 5). The spectral maxima of the SHG directly connected with the nonlinear optical susceptibilities (NLO) are clearly observed. From eqs 2a and 2b, it is clear that nonlinear optical electron−phonon cascading processes are responsible for the observed phenomena. For deeper understanding of the processes, we have measured spectral dependences of intensities of the anharmonic phonon modes at different IR-inducing powers (see Figure 6). Comparing Figures 5 and 6, one can see a correlation between the IR-induced anharmonic phonon maxima and the output SHG intensities. This is an additional argument confirming theoretical predictions about the dominant role played by the photoinduced anharmonic EPI.

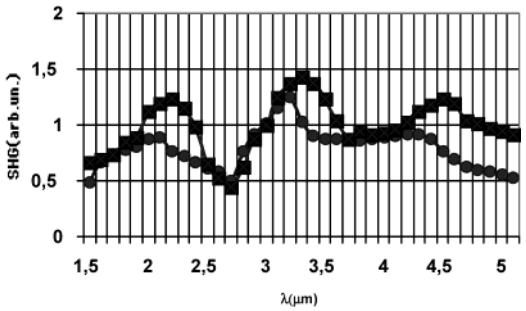

Figure 5. Spectral dependence of the fifth-order nonlinear optical susceptibility ($\chi^{(5)}$) in $\times 10^{-40}$ m^4/V^4 SHG at different IR-induced CO laser intensities: (●) 0.5 GW/cm^2; (■) 0.8 GW/cm^2.

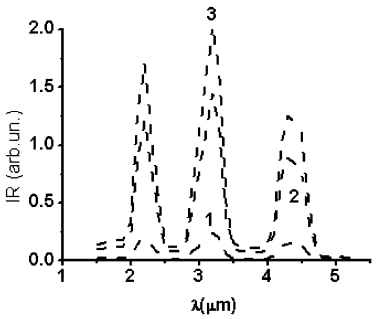

Figure 6. Photoinduced spectral dependences of the IR modes at different CO laser powers: (1) 0.25 GW/cm^2; (2) 0.50 GW/cm^2; (3) 0.80 GW/cm^2.

The observed IR poling consists of the simultaneous presence of the fifth-order steady-state nonlinear optical quantum cascading processes and the IR-induced charge density noncentrosymmetry. The first condition is achieved because of the close values of the IR-induced frequencies and IR energy gaps. The second one is caused by induction of charge density anisotropy due to IR-induced anharmonic phonons.

Experimentally, the first effect may be manifested through the spectral dependences of the SHG intensities versus the anharmonic phonon frequencies. The second one may be displayed through the monitoring of the pump−probe nonlinear optical kinetics occurring at delay time about 20 ps, contrary to the ultrafast pure electronic relaxation time (below 1 ps) during the usual steady-state process.

Conclusions

The IR-induced fifth-order SHG in halcogalide Sb_2Te_3−BaF_2−$PbCl_2$ glasses was experimentally observed. The main difference of the present cascading fifth-order nonlinear optical effect compared to the traditional second-order one consists of substantial contribution of anharmonic electron−phonon subsystems induced by the IR pumping power. Independent measurements of the photoinduced IR spectra confirmed additionally a good agreement between spectra of the photoexcited IR modes and the output SHG. The relaxation kinetics of these effects is consistent with a simple model of electron−phonon anharmonic interactions. The technique described may be used quite generally in IR optical fibers and may be applied to a wide variety of IR-inducing processes including two-photon absorption, nonlinear optical parametric generations, and nonlinear cascading exciton−phonon interactions. The IR-induced SHG opens surely new possibilities in the tailoring of phase-matching glasses for the IR frequency conversion.

Acknowledgment. The work is done within Grant GU3 WMP 39-00 of the Polish Committee of Science.

References and Notes

(1) Bloembergen, N. *Nonlinear Optics*; Benjamin: New York, 1965. Boyd, R. W. *Nonlinear Optics*; Academic: Boston, 1992.

(2) Chemla, D. S.; Zyss, J. *Nonlinear Optical properties of Organic Molecules and Crystals*; Academic: New York, 1986; Vols. 1 and 2.

(3) Homoelle, D.; Wielandy, S.; Gaeta, A. L.; Borelli, N. F.; Smith, C. *Opt. Lett.* **1999**, *24*, 1311. Grubsky, V.; Feinberg, J. *Opt. Lett.* **2000**, *25*, 203. Stegall, D. B.; Erdogan, T. *J. Opt. Soc. Am.* **2000**, *17A*, 304.

(4) Dodge, J. S.; Schumacher, A. B.; Bigot, J.-Y.; Chemla, D. S.; Inglr, N.; Beasley, M. R. *Phys. Rev. Lett.* **1999**, *83*, 4650. Gautier, C. A.; Lefumeux, C.; Albert, O.; Etchepare, J. *Opt. Commun.* **2000**, *178*, 217.

(5) Antonyuk, B. P. *Opt. Commun.* **2000**, *181*, 191.

(6) Charra, F.; Kajzar, F.; Nunzi, J. M.; Raimond, F.; Idiart, E. *Opt. Lett.* **1993**, *18*, 941. Primozich, N.; Shahbazyan, T. V.; Perakis, I. E.; Chemla, D. S. *Phys. Rev.* **2000**, *61B*, 2041.

(7) Zhao, X.; Xu, L.; Yin, H.; Sakka, S. *J. Non-Cryst. Solids* **1994**, *167*, 70. Kityk, I. V.; Kasperczyk, J.; Plucinski, K. *J. Opt. Soc. Am.* **1999**, *16B*, 1719.

(8) Kityk, I. V.; Sahraoui, B. *Phys. Rev. B* **1999**, *60*, 942.

(9) Hisakuni, H.; Tanaka, K. *Appl. Phys. Lett.* **1994**, *65*, 2925. Schaafsma, D. T.; Shaw, L. B.; Cole, B.; Sanghera, J. S.; Aggarwal, I. D. *IEEE Photonics Technol. Lett.* **1998**, *10*, 1548. Frumar, M.; Polak, Z.; Cernosek, Z. *J. Non-Cryst. Solids* **1999**, *257*, 105. Wasylak, J.; Kucharski, J.; Kityk, I. V.; Sahraoui, B. *J. Appl. Phys.* **1999**, *85*, 425. Quiquempois, Y.; Villeneuve, A.; Dam, D.; Turcotte, K.; Muller, J.; Stegeman, G.; Lacroix, S. *Electron. Lett.* **2000**, *36*, 733. Churikov, V. M.; Valeyev, A. I.; Shavelev, K. O.; Shavelev, O. S. *Opt. Mater.* **2002**, *19*, 415; **2000**, *14*, 69.

(10) Dalal, N.; Klymachyov, A.; Bussmann-Holder, A. *Phys. Rev. Lett.* **1998**, *81*, 5924. Geller, M. R.; Dennis, W. M.; Markel, V. A.; Patton, K. R.; Simon, D. T.; Yang, H. S. *Physica* **2002**, *B316*−*317*, 430.

(11) Napieralski, J. *Ferroelectrics* **1999**, *220*, 17.

(12) Fiorini, C.; Charra, F.; Nunzi, J.-M. *J. Opt. Soc. Am.* **1994**, *11B*, 2347.

(13) Mostepanenko, S. Ph.D. Thesis, Moscow Technical University, Moscow, Russia, 1998; p 235.

(14) Davydov, A. S. *Introduction to the Solid State Physics*; Nauka: Moscow, 1997 (in Russian).

(15) Bachelet, G. B.; Hamann, D. R.; Schluter, M. *Phys. Rev.* **1982**, *26B*, 419. Kityk, I. V.; Kasperczyk, J.; Andrievskii, B. V. *Phys. Lett. A* **1996**, *216*, 161.

(16) Sahraoui, B.; Kityk, I. V.; Nguyen Phu, X.; Hudhomme, P.; Gorgues, A. *Phys. Rev.* **1999**, *59B*, 9229.

(17) Etile, A.-C.; Fiorini, C.; Charra, F.; Nunzi, J.-M. *Phys. Rev.* **1997**, *56A*, 3888.

(18) Melancholin, A. *Principles of measurements in the crystallooptics*; Nauka: Moscow, 1974 (in Russian).

(19) Maker, P. D.; Terhune, R. W.; Nisenoff, M.; Savage, C. M. *Phys. Rev. Lett.* **1962**, *8*, 41.